Managing Surface Operations of Lunar South Pole and Optimizing PSR Pathfinding Plans

Ronald H. Freeman, PhD
Space Operations & Support Technical Committee, AIAA

Introduction

An Artemis III landing site and Artemis Base Camp within 6° of the lunar south pole (LSP). will be in an impact-cratered terrain occurring at all scales, from micrometers to >1000 km. This cratering produces PSRs, the areas where science teams are especially interested in collecting data. It would be impossible for an astronaut to take a single step on the Moon without stepping into or onto an impact crater [1]. In terms of surface features, the area most resembles the highland terrain explored in the Apollo 16 mission, as shown in Figure1.

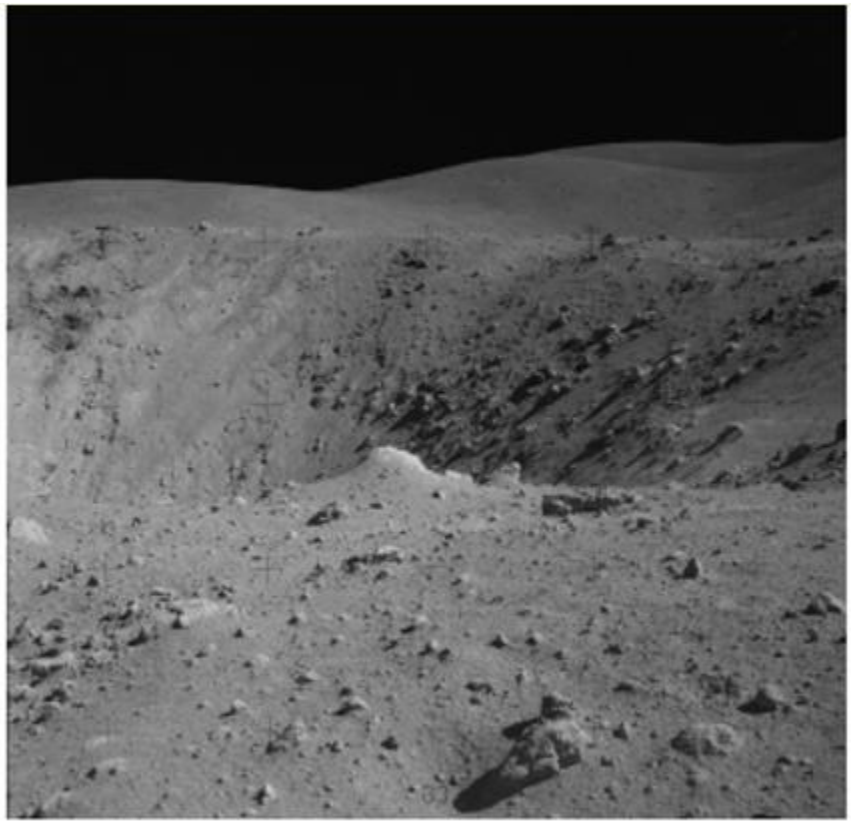

Figure 1. Apollo 16 Highlands Terrain at North Ray Crater

The Lunar Reconnaissance Orbiter (LRO) camera image of Apollo 16 Highlands Terrain at North Ray Crater provides a resolution of 5m imagery as well as terrain elevation data. Further analysis of imagery reveals the movement of shadows in multiple images of the same sites and provides a capability to determine size and position of boulders and craters smaller than 5m down to about 1m. Images of emerging LSP distributions of rocks and small craters align with previously established distributions provided in the Cross-Program Design Specification for Natural Environments [2]. Due to extremely low solar incidence (grazing sunlight just above the horizon) and large local topography variations, LSP areas exist in permanent shadow (Permanently Shadowed Regions, or PSRs), that receive either no direct sunlight or minimal scattered light from surrounding areas. Based on the accumulated polar imagery from the LRO – WAC camera, the current highest resolution time-weighted illumination maps (South Pole) are shown in Figure 2 [3].

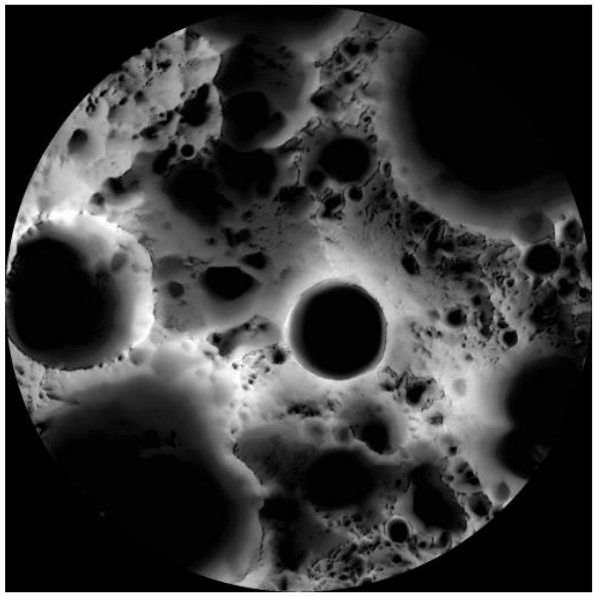

Figure 2. Multi-temporal illumination map of the lunar south pole, Shackleton crater (19 km diameter) is in the center, the south pole is located approximately at 10 o'clock on its rim. Mapped area extends from 88°S to 90°S [NASA/GSFC/Arizona State University].

Bombardment early in the Moon's development, allowed sufficient time for the accumulation of regolith to bury most of the ejecta and transform small craters into a hummocky, or humpy surface [4]. Therefore, Artemis lunar surface operations will require skills for longer duration missions and more sustained lunar operations including

- Basic crew geologic training and EVA simulations in appropriate analogue terrains.
- Complex mission simulations conducted in analogue terrains with the integrated expertise of the astronaut office, astronaut trainers, field geology trainers, site selection teams, geologists involved in surface operations planning, lunar sample analysts, in situ resource specialists when appropriate, equipment designers, flight controllers, and management. Simulations uncover unanticipated challenges, produce a well-working team with resiliency to successfully resolve unexpected conditions during a lunar surface mission.

Lunar Roving Vehicles (LRV) launched on Apollo 15, Apollo 16, and Apollo 17, enabled astronauts to explore a greater area and collect more distant samples than possible by foot. The LRV had no autonomous maneuvering capabilities and struggled to stay in contact with flat ground when traveling more than 9 mph. In addition, astronauts were range limited as they could not drive further from the lunar lander than they could walk. This limitation was a safety feature to prevent them from becoming stranded in the event of a LRV mechanical failure [5]. Apollo missions pursued a diverse set of scientific and exploratory objectives. Relevant tasks often required astronauts to embark on lengthy traverses across the inhospitable lunar landscape. Such EVA operations met considerable challenges, adversely affecting both astronaut safety and performance. The most immediate obstacle hampering lunar navigation stemmed from the distinct illumination on the Moon. Apollo astronauts reported difficulties arising from poor color contrasts, intense surface reflections. Conversely, areas covered in pitch-black sharp shadows (a result of the Moon's lack of atmosphere) complicated object identification and obstacle avoidance, making tripping hazards an ever-present concern. The absence of atmospheric light scattering likewise contributed to impaired distance and size estimation, to cause objects fappear closer than they actually were. NASA's Preliminary Science Report for the Apollo 11 mission described the lunar terrain as "steep slopes, deep holes, and ridges." The lack of natural vertical features, combined with unclear horizon definition and weak gravity cues at the observer's feet, were also blamed for "difficulties in identification of level areas when looking down at the surface" [6].

Figure 3. Astronaut Edgar Mitchell using a paper traverse map to navigate on the lunar surface during Apollo 14 (left). Astronaut Charles Duke on the edge of the Plum Crater (middle). Buzz Aldrin egressing the lunar lander during Apollo 11 (right). The pictures underscore the difficult terrain and lighting conditions that astronauts need to face during EVAs on the lunar surface, such as pitch-black shadows and blinding sunlight. Credit: NASA.

Due to communication delays between Earth and the Moon, along with frequent radio blackouts, a high level of astronaut autonomy will likely be required. Confronted with these challenges, the use of head-up displays (HUDs) along with relevant technologies, such as Augmented Reality (AR), promises to superimpose contextually relevant information over the user's view of the real world. These solutions benefit astronauts in surficial terrain navigation and pathfinding [7]. HUD solutions have already been successfully utilized to enhance the perception and situational awareness of soldiers [8]. Headworn displays featuring tracking capabilities have been employed to spatially overlay points of interest in the real world with AR navigational cues. A number of benefits to such a practice includes enhanced performance (likely due to a reduced visual scanning time and reduced visual clutter, enhanced integration of user information, and reduced attention capture [9]. Some prototypes have found their way into analogue testing and training activities. For instance, the Microsoft HoloLens 2 HMD has been employed to provide navigational guidance during an analogue mission near the Kilauea volcano. Notably, participants in the study voiced their preference for the experimental HUD over traditional navigational devices, citing its superior legibility under direct sunlight. In the same analog mission setting, the feasibility of utilizing HUDs to visualize optimal traversal paths in challenging terrains was demonstrated by Anandapadmanaban et al. [10]. Building on this foundation, Bonilla et al. (2022) proposed a prototypical AR-based obstacle avoidance system [11] with suggested requirements:

1. In contrast to the Apollo rover, LRVs for the Artemis program will have to advance robotic capabilities. Under support from the NASA Moon-to-Mars X-Hab program, University of Maryland is developing a robotic roving vehicle concept for lunar use with Earth analog testing and evaluation. Probabilistic risk assessments indicate a greater utility for two vehicles designed for nominal single-person use, but each capable of carrying a second EVA crew in the event of a vehicle failure. This mitigates the Apollo-era stringent "walk-back" criteria, which limited both overall traverse distance and allowable exploration time at remote sites.
2. Rovers shall have a maximum operating speed of at least 4 m/sec on level, flat terrain.
3. Rovers shall be designed to accommodate a 0.3 m obstacle at minimal velocity.
4. Rovers shall be designed to accommodate a 0.1 m obstacle at a velocity of 2.5 m/sec.
5. Rovers shall be designed to safely accommodate a 20° slope in any direction at a speed of at least 1 m/sec and include the ability to start and stop – The Lunar Exploration Science Working Group study of 1995 found that, for general access to anywhere on the moon, rovers should be capable of ascending and descending a 25° slope.
6. Rovers shall have a nominal sortie range of 54 km at an average speed of 2.5 m/sec, equivalent to six hours of constant driving on level terrain at 2.5 m/sec.
7. Rovers shall be capable of carrying one 170 kg EVA crew and 80 kg of assorted payload under nominal conditions – The nominal mass of the EVA crew was based on an 80 kg astronaut and a 90 kg spacesuit/life support system.
8. Payload may be modeled as a 0.25 m^3 box – This is a minimal constraint to ensure some space on the rover deck for payload.
9. Rovers shall be capable of also carrying a second 170 kg EVA crew in a contingency situation.

10. Rover design shall incorporate roll-over protection for the crew and all required ingress/egress aids and crew restraints, absent on the Apollo LRV.
11. A nominal sortie shall be at least eight hours long.
12. Two rovers must be launched on a single CLPS lander.
13. A single rover shall have a mass ≤ 250 kg, based on Astrobotics Griffin rover's 500 kg payload limit.
14. Rovers shall be developed in time to be used on the first Artemis landing mission.
15. Rovers shall be capable of operating indefinitely without crew present for recharging in situ.
16. Rovers shall be capable of direct, remote, or automated operations.
17. Rovers shall be capable of following an astronaut, following an astronaut's path, or autonomous path planning between waypoints.
18. Rovers shall be capable of operating during any portion of the lunar day/night cycle and at any latitude in order to not preclude rover use regardless of landing site or duration

Problem

A key to mission success will be accessing promising stations identified in pre-mission mapping. Owing to locally heterogeneous slopes, large elevation changes, and low illumination, challenging EVAs require automating the initial assessment of a large number of potential targets for pre-planning traversal routes. Astronauts will have to navigate the desolate and achromatic lunar landscape, characterized by extreme lighting conditions, while grappling with the constraints of their bulky space suits, limited mobility and field of vision, expected to cause high fatigue, poor situational awareness, and impaired spatial orientation [13]. Steep undulating slopes pose a challenge for walking EVAs anticipated for the Artemis III and subsequent missions. Using 5 m/pixel Lunar Orbiter Laser Altimeter (LOLA) measurements of the surface, an automated Python pipeline was developed to calculate traverse paths that minimize metabolic workload. The tool combines a Monte Carlo method with a minimum-cost path algorithm that assesses cumulative slope over distances between a lander and stations, as well as between stations. To illustrate the functionality of the tool, optimized paths to permanently shadowed regions (PSRs) were calculated around potential landing sites 001, nearby location 001(6), and 004, all within the Artemis III 'Connecting Ridge' candidate landing region [14]. Some polar regions of the Moon contain areas have never experienced sunlight. Because of the complex LSP topography where the Sun never rises more than a few degrees above the horizon, long shadows stretched across the surface. To access PSRs, the strength of the soil must be known at these locations for safe traversals. Thirteen LSP boulder tracks were identified on the edge of, or within PSRs using images taken by the Lunar Reconnaissance Orbiter. The images were processed to enable the measurement of boulders and their associated tracks. The tracks identified within PSRs have similar appearances to those identified outside PSRs in other regions on the Moon.

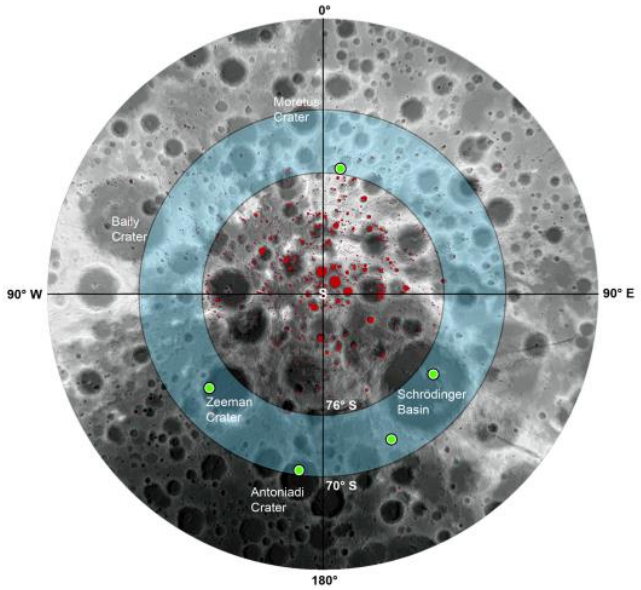

Figure 4a. A south polar view of the Moon with permanently shadowed regions (PSRs) highlighted in red [McGovern, J. A., Bussey, D. B., Greenhagen, B. T., Paige, D. A., Cahill, J. T., & Spudis, P. D. (2013). Mapping and characterization of nonpolar permanent shadows on the lunar surface. Icarus, 223(1), 566–581] and the location of

identified PSR boulder tracks in green. The blue band area represents the region where boulder tracks were observed in PSRs, located between ~70° and 76° latitude, that is, the region where secondary illumination and image processing still allow to use NAC images without compromising spatial resolution.

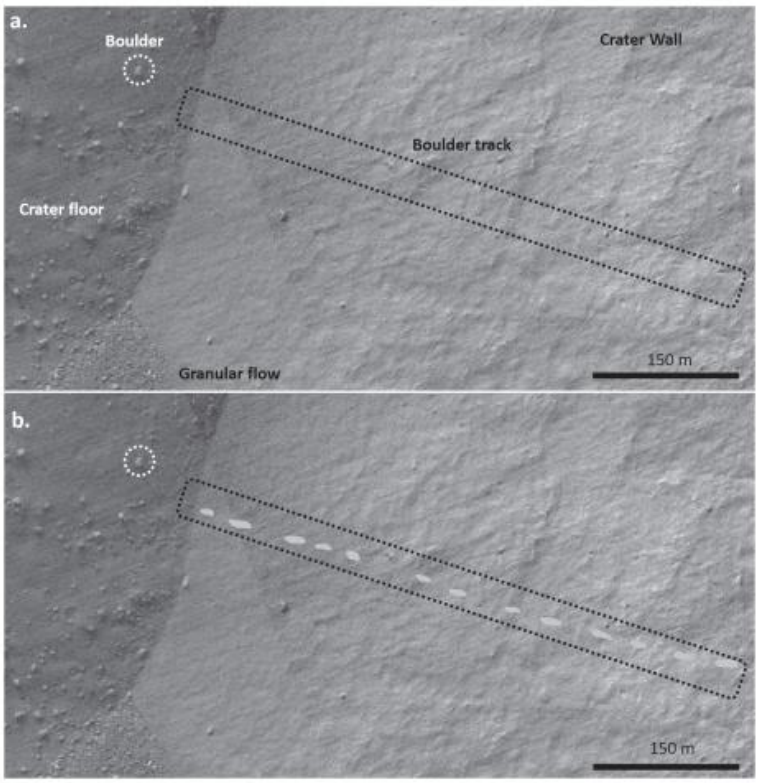

Figure 4b. An example of a boulder track and boulder identified in a permanently shadowed region. The entire image is inside a permanently shadowed region that covers the crater floor and wall. The image is a detail of a filtered Narrow Angle Camera (NAC) image M1117841678R inside an unnamed crater at latitude −72.219° and longitude 154.671°. Image (a) shows the unmarked track, and image (b) shows the highlighted track.

The strength of soil within PSRs was estimated from the measurements taken and was shown to be at least as strong as highland and mare regions of the Moon at relatively shallow depths. Analysis shows that PSRs of the type measured should be able to bear rovers at depths of at least ~30 cm. In situ measurements are required to confirm and better understand the mechanical behavior of PSR regolith at shallow depths [15]. 521 PSRs were identified. Traverse paths to accessible PSRs were computed within 2 km of the landing sites, and descents from host crater rims into each PSR were optimized. Slopes were limited to 15° and previously identified boulders were avoided. Surface temperature, astronaut body illumination, regolith bearing capacity, and astronaut-to-lander direct view were simultaneously evaluated. A total of 20 and 19 PSRs are accessible from sites 001 and 001(6), respectively, four of which maintain slopes <10°. Site 004 provides access to 11 PSRs, albeit with higher EVA workloads. From the crater rims, 94 % of PSRs are accessible. And, all roundtrip traverses from potential landing sites can be performed under 2 h. In the context of rover routing design, developing algorithms aims find the optimal path between two points on a map.

With available topographic data up to 5 m/pixel resolution for elevation and slope, minimum-cost calculation algorithms provide optimal traverses of reduced distance traveled as well as lowered risk from high slopes. Dijkstra's algorithm computes traverses that minimize the metabolic workload for a specified illumination condition. Dijkstra's algorithm produces a shortest-path tree from the starting point (landing site or crater rim) to the endpoint (PSR edge or center), allowing both lateral and diagonal movements between adjacent pixels [16]. The 5 m/pixel LOLA Digital Slope Model (LDSM) data is employed as a cost map, using cumulative slope as the optimization metric. The ‘best’ traverse is chosen by evaluating the lowest cumulative slope result. The algorithm intrinsically considers distance and height. Height is considered in the slope (as the cumulative slope is assessed), therefore a

greater elevation change over a set distance implies a higher slope (worsening the cumulative slope result). Per graph representation as an adjacency matrix, i.e., a regular and gapless structure, the algorithm effectively balances the trade-off between distance and elevation change, resulting in traverses that minimize the cumulative slope and, consequently, the metabolic workload. Figure 5 shows a comparison between the path generated by the path-finder algorithm and two alternative paths created by users. The users manually smoothed the paths and introduced detours based on visual inspection of NAC images. While the automated traverse may be slightly longer, the significant reduction in metabolic workload achieved through lower cumulative slopes ensures optimal energy management during EVAs.

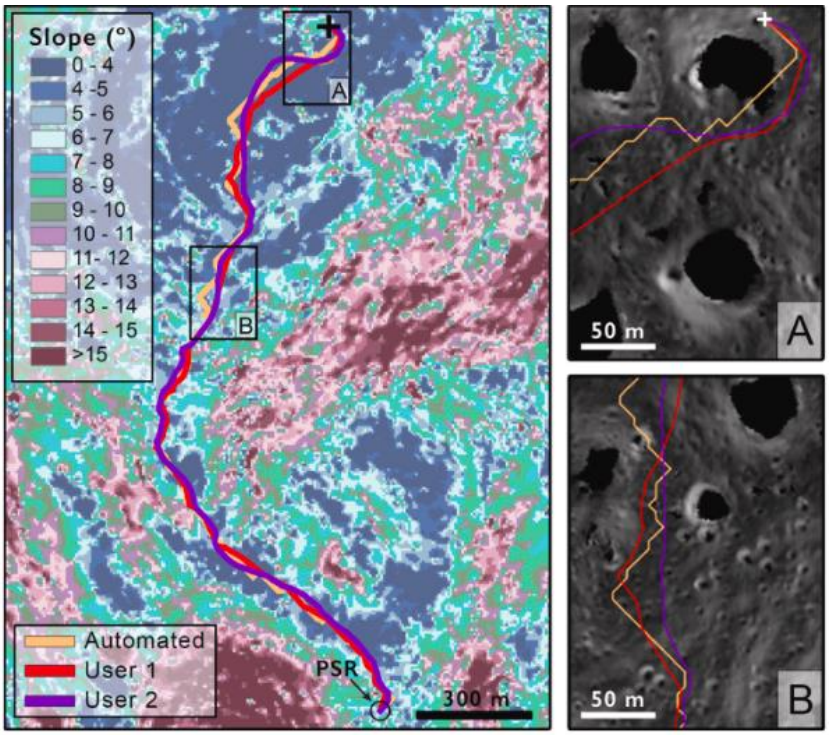

Figure 5. Comparison of traverses to PSRs between two user-drawn paths and path-finder algorithm result. Left panel shows the traverses overlaid on the slope map. Right panels show the traverses overlaid on NAC images.

Purpose

In the dynamic path-planning environment for lunar rovers, actions may fail due to unforeseen situations, such as navigating at low speeds or traversing novel pathways, particularly in instances where rovers encounter restricted visibility. This paper aims to explore how lunar surface rovers perceive and respond to surrounding LSP environment in real time and how local path planning assist in optimizing their respective lunar operations.

Methods and Results

A new collaborative path-planning method based on deep reinforcement learning includes heuristics that lead rovers to move without obstacles, finish rovers' tasks, and reach different targets. An imperative challenge lies in devising a sequence of actions to guide rovers toward their targets within partially unknown environments. Automated Scheduling and Planning Environment (ASPEN), formulated by NASA, generated activity sequences for one spacecraft with constraints on resources and operating rules. Japan Aerospace eXploration Agency (JAXA) has introduced a path-planning algorithm that prioritizes decision-making specific to the limitations of sunlight rather than simply avoiding obstacles. And a GPS-based path planning algorithm is proposed for rovers to generate paths in difficult terrain although the mature positioning system for lunar environments has yet to be developed [17].

Typically image-based, aerial and/or rover imagery is used with computer vision methods to identify rocks and craters as obstacles. Most approaches generate grid-based maps from this data with the objective of rovers avoiding obstacles, and some incorporate terrain mapping to grade the traversability as poor, low, moderate, or high [18]. For example, a rover might need to identify hazardous obstacles in a timely manner. Therefore, simultaneous location

and mapping (SLAM)-based robotic mapping systems employ a variety of image sensors. Active sensors (e.g., LiDAR, radar, and time-of-flight camera) directly obtain 3D topographic data regardless of dark illumination conditions. However, for a solar panel- and battery powered- rover, active sensors are heavy, large, and have high energy consumption. Therefore, most rovers for Moon and Mars explorations carry optical cameras (passive sensors) due to their lighter weight, smaller size, and lower power consumption. LOLA-based digital elevation models (DEM) inform traversals with surface elevations and topographical properties of polar regions but are less helpful with rovers determining obstacle-free, shortest distance, and least energy-consuming paths. Future robotic missions require rovers to autonomously navigate and map uncertain environments. Local DEMs and digital orthophotos of landing site or traversed areas generate images for feature matching and bundle adjustments to adjacent images along traverses [19].

In the dynamic path-planning environment for lunar rovers, actions may fail due to unforeseen situations, such as navigating at low speeds or traversing novel pathways, particularly in instances where rovers encounter restricted visibility. The absence of direct sunlight in PSRs challenges robotic operations to obtain clear images, consequently impacting crucial tasks such as obstacle avoidance, pathfinding, and scientific investigation. In a visual simultaneous localization and mapping (SLAM)-based robotic mapping, low-light image enhancement (LLIE) methods leverage scattered low light to enhance the quality and clarity of terrain images, resulting in an overall improvement of brightness and contrast of images captured in poorly exposed regions, thus enhancing the capability of the robotic mapping method to estimate the location of a rover and to construct a topographic map of its surroundings. Methods that characterize intensity values in a given image, refine the illumination to enhance the image. By separately adjusting illumination and reflectance components, the image is enhanced [20]. Reflectance of an image remains constant regardless of lighting conditions, whereas illumination represents varied lighting conditions [21]. Wang, et al. (2018) considered first calculating a global illumination estimation for the low-light image, then adjusting the illumination guided by the estimation and uses a concatenation with the original image to enhance details [22]. Their global illumination-aware and detail-preserving network (GladNet) consisted of two steps. In order to obtain a global illumination prediction, the image is first down-sampled to a fixed size and passed through an encoder-decoder network (e.g., global illumination estimation step). The bottle-neck layer of the encoder-decoder has a receptive field that covers the whole image. The second step entails a detail reconstruction step to supplement the details lost in the rescaling procedure. Training such a network utilizes a synthesized training dataset of 780 raw images from a large dataset of 8156 high-resolution raw images (or, RAISE): 700 for generating pairs for training and 80 for validation [23]. As shown in Figure 6, the global illumination estimation step down-samples inputs to a fixed size. Then, feature maps are passed through an encoder-decoder network. At the bottle-neck layer, the global illumination is estimated. After scaling back to the original size, an illumination prediction for the whole image is obtained. The global illumination estimation step is followed by a detail reconstruction step. Three convolutional layers adjust the illumination of the input image referring to the global-level illumination prediction and fill in the details lost in the down-sampling and up-sampling procedure at the same time.

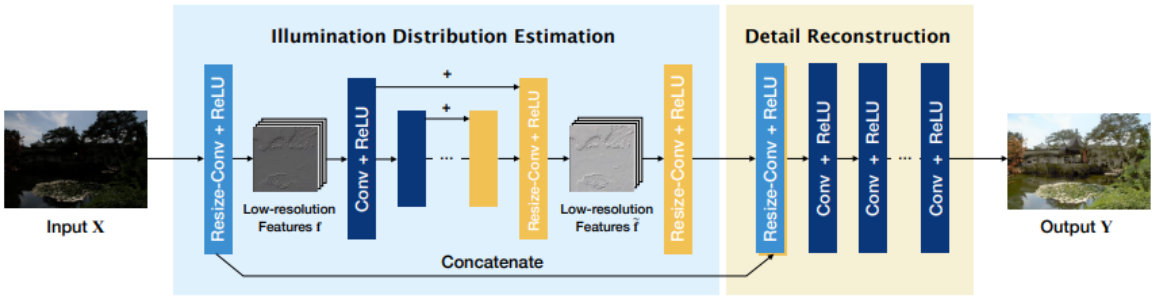

Figure 6. The architecture of GladNet. The architecture consists of two steps, global illumination estimation step and detail reconstruction step. In the first step, the encoder-decoder network produces an illumination estimation of a fixed size (96 × 96 here). In the second step, a convolutional network utilizes the input image and the outputs from the previous step to compensate the details.

The visual SLAM-based robotic mapping method was designed for building a highly detailed 3D point cloud map in the lunar PSRs. Unlike other planetary robotic missions during daytime, a low-illumination condition in the PSRs

degrades the quality of image pairs from the stereo camera mounted on a rover. Low visibility, color distortion, and increased noise lead to erroneous rover trajectories and mapping results. Therefore, in the preprocessing thread, the LLIE method is additionally utilized to enhance mapping capabilities and visual perception and tracking. In the mapping process, all point clouds from every key frame are re-projected onto a coordinate system from the first frame in an image sequence. The mapping space is divided into a set of 3D grids with a predefined resolution. Each grid referenced in a 3D coordinate system registers several 3D points and their RGB pixel color information. The 3D grid helps in filtering and managing point clouds.

The fundamental difference between an image and a point cloud is that the point cloud is a 3D representation of an environment whereas an image is a 2D representation (or, at best, a "two and a half" dimensional representation). A second major difference is that images are most typically represented using a uniform grid structure whereas a point cloud allows a non-uniform point (or "sample") spacing. Since the grid is a uniformly spaced structure, only values at the grid intersections are stored the (for example, Z for an elevation raster or Red-Green-Blue values for an image). On the other hand, the point cloud with randomly distributed values and all coordinates are stored (for example, X, Y, Z and perhaps other values as well). In general, an image is a compact way of representing a 2D view of an object (such as a digital orthophoto) whereas the point cloud is useful for a richer, fully 3D view. An image allows planimetric measurements (for example, how far one intersection is from another without regard to height differences). A point cloud allows fully 3D measurements [Graham, L. (2013). Point clouds from images. *Lidar Magazine*].

Figure 7 shows the overall flow of the proposed method consisting of three main threads: preprocessing, localization, and dense mapping.

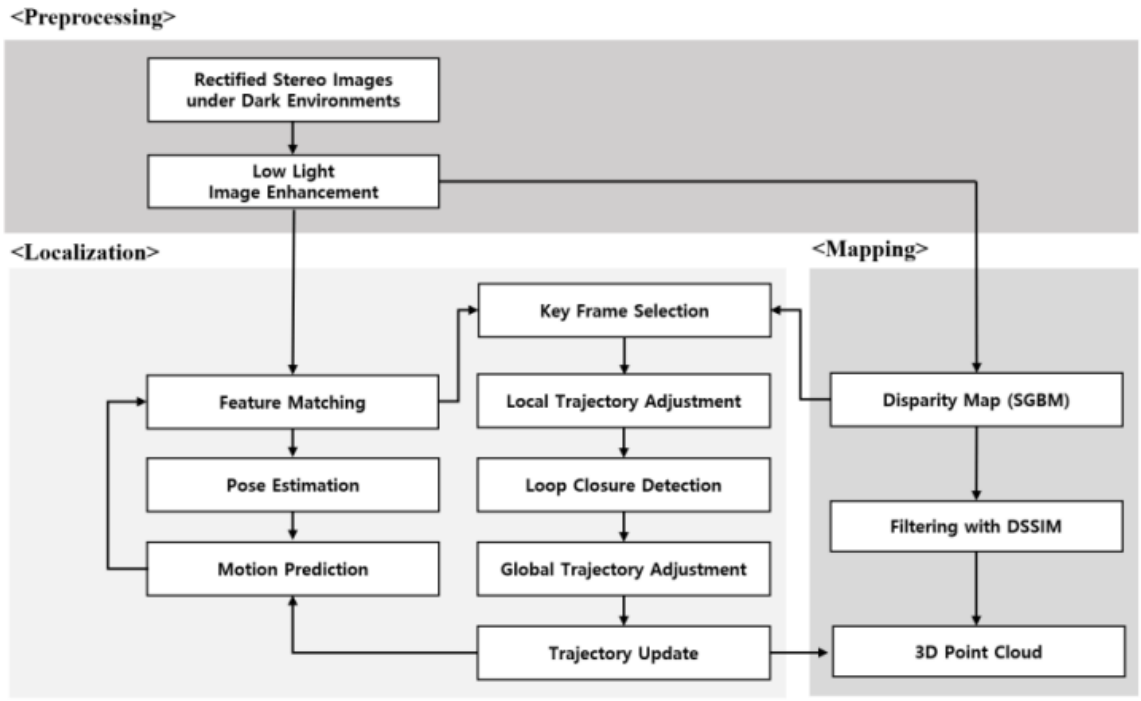

Figure 7. Overall flow of the robotic mapping method.

Enhanced images inevitably have color alterations and information loss, a source of potential errors that creates noise in a 3D point cloud. Thus, structural dissimilarity (DSSIM), a distance metric derived from the structural similarity index measure (SSIM) [24], is used as a filter to examine a pixel-wise correspondence between stereo pairs and to increase mapping accuracy. Since accuracy of a disparity estimate is lower at longer distances, only 3D points closer than a predefined distance (e.g., 5 m) are mapped. In the mapping process, all point clouds from every

key frame are re-projected onto a coordinate system from the first frame in an image sequence. The mapping space is divided into a set of 3D grids with a predefined resolution. The 3D grid helps in filtering and managing point clouds. The localization thread adopts stereo parallel tracking and mapping (S-PTAM) [25] as a base framework for estimating a camera's pose and trajectory by matching the correspondences between a terrain feature and identical features on the stereo image keyframe (Figure 6). The following keyframe is selected if the number of feature matches is less than 90% of that in the previous keyframe. And, that keyframe is used to update the camera pose by triangulating between feature matches of neighboring frames. Although low-light enhanced images from the preprocessing thread increase the quality and quantity of feature matches [26], feature extraction and matching method is limited to homogeneous (textureless) terrains in the PSRs.

Analogue testing and training activities provide navigational guidance in an analogue terrain for the employment of LLIE and GladNet methodologies. Under dark conditions without LLIE methods, a 3D terrain fails to be reconstructed due to insufficient number of feature matches. However, when combined with GladNet, stereo image pairs from the rover-mounted camera are sequentially enhanced, the result is a significant improvement in both quantity and quality of feature matches. Moreover, the restored color information combined with the depth value in the disparity map produces point clouds with consistent brightness and color. The point cloud map shows sparse density in the middle and reveals occlusions at nearby craters/ rocks due to the low tilting angle of the stereo camera mounted on the rover's mast. However, the colorized 3D points helps to better understand morphological characteristics of craters and mounds. Furthermore, rocks and pebbles with different colors are clearly identified, along with their respective sizes and shapes [27].

Discussion and Conclusion

Future lunar exploration for teams of astronauts and rovers will be enhanced through the use of augmented reality (AR) for the purpose of navigating a planned traverse. Wrist displays and tablets have long been standard tools for navigation and used for analog planetary EVA traverses. However, they distract the astronaut from their environment as the astronaut repeatedly looks at the display leading to the potential for loss of situational awareness. More primitive navigation methods, such as guidance through voice commands from mission control, may distract the astronaut's focus from exploring the environment. Nonetheless, robotic exploration of lunar PSRs has not yet been achieved. There are no direct measurements of illumination available, even for PSR pathfinding transversal routes. It is expected that the actual illuminance levels will vary significantly depending on factors such as topography, nearby terrain features, and the specific location within PSRs. Also, the illumination and terrain conditions in the testbed are limited to emulate the large-scale and complex environment of PSRs. Since camera imagery varies due to time of day, electronic component heating, and model of camera and lens, the resultant image effects are difficult to discern with high degree of certainty; enhanced illumination makes for better simulated-based predictions in analogue terrains. Vision-based pose estimation using deep learning offers a promising cost effective and versatile solution for relative satellite navigation purposes. Relying on feature extraction and a deep neural network that affords learning of data [28], a deep reinforcement learning framework models adaptive decision-making, as it leverages the ability of an agent to autonomously interact with the environment. However, the validation task entails bridging the gap between the dataset and real-world data. In the context of lunar operations, gathering a vast amount of real-world data is prohibitively expensive. This lack of data inspires developing new validation techniques, both for the constitution of more representative synthetic datasets and for the correct quantification of the proposed lunar architecture performances. With respect to user distance z from the target (i.e. PSR), errors depend on the geometrical definition of the problem, e.g., dependence on the object shape, on the angular field of view of the camera and its resolution. Current pose (e.g., altitude and position) estimation techniques can be categorized in two types of approaches: direct approaches (predicting directly orientation and relative position of the target object) and indirect approaches (predicting intermediate representations). Real images taken on the ground are important for assessing robustness to domain gap. From validation and performance verification viewpoint, lunar pathfinding in difficult terrains is challenging. Space applications (e.g. on-orbit rendezvous) require generation of synthetic datasets. For space rendezvous, performance improves relative to distance with trajectory convergence and mitigation of collision risks. Even if representative space is generally limited, testing on a robotic test bench is clearly a mandatory step to validate a pose estimation solution, thus providing robustness to the corresponding change of domain. Existing dataset is complemented with a subset of real images of space scenes produced using a robotic testbed. Data augmentation and domain adaptation techniques help limit performance degradation in disturbed conditions. Moreover, the addition of numerous metadata allows deeper investigation into multi-tasking and multi-modal architectures.

References

[1] Null, C. H., Kaiser, M. K., Wolters, T. E., Marquez, J. J., Cooter, A. M., & Dischinger Jr, H. C. (2023, May). Identification of Risks to Eva Created By Ambient Lighting Conditions at the Lunar South Pole. In *12th International Association for the Advancement of Space Safety (IAASS) Conference* (No. 202300000821)].

[2]Cross-Program Design Specification for Natural Environments, (DSNE), Revision I (2021), NASA Document # SLS-SPEC-159].

[3]Speyerer, E. J., & Robinson, M. S. (2013). Persistently illuminated regions at the lunar poles: Ideal sites for future exploration. *Icarus*, *222*(1), 122-136.).

[4]Cross-Program Design Specification for Natural Environments, (DSNE), Revision I (2021), NASA Document # SLS-SPEC-159].

[5]Williams, D. The Apollo Lunar Roving Vehicle. Retrieved from NASA.gov].

[6] Bensch, L., Nilsson, T., Wulkop, J., de Medeiros, P., Herzberger, N. D., Preutenborbeck, M., ... & Cowley, A. (2024). Designing for Human Operations on the Moon: Challenges and Opportunities of Navigational HUD Interfaces. *arXiv preprint arXiv:2402.15692*]

[7]Paul de Medeiros, Paul Njayou, Flavie Rometsch, Tommy Nilsson, Leonie Becker, and Aidan Cowley. 2022. Categorisation of future applications for Augmented Reality in human lunar exploration. In Proceedings of the International Astronautical Congress, IAC. Paris, Frankreich].

[8]Mark A. Livingston, Lawrence J. Rosenblum, Dennis G. Brown, Gregory S. Schmidt, Simon J. Julier, Yohan Baillot, J. Edward Swan, Zhuming Ai, and Paul Maassel. 2011. Military Applications of Augmented Reality. In Handbook of Augmented Reality, Borko Furht (Ed.). Springer, New York, NY, 671–706.].

9]Christopher D Wickens and Jeffry Long. 1995. Object versus space-based models of visual attention: Implications for the design of head-up displays. Journal of Experimental Psychology: Applied 1, 3 (1995), 179]

[10]Eswar Anandapadmanaban, Jesslyn Tannady, Johannes Norheim, Dava Newman, and Jeff Hoffman. 2018. Holo-SEXTANT: an augmented reality planetary EVA navigation interface. 48th International Conference on Environmental Systems]

[11] Angelica M Bonilla Fominaya, Rong Kang Chew, Matthew L Komar, Jeremia Lo, Alexandra Slabakis, Ningjing Sun, Yunyi Zhang, and David Lindlbauer. 2022. MoonBuddy: A Voice-based Augmented Reality User Interface That Supports Astronauts During Extravehicular Activities. In Adjunct Proceedings of the 35th Annual ACM Symposium on User Interface Software and Technology. 1–4]

[12] Akin, D., Hanner, C., Bolatto, N., Gribok, D., & Lachance, Z. (2021, July). Design and Development of an EVA Assistance Roving Vehicle for Artemis and Beyond. 50th International Conference on Environmental Systems]:

[13Kristine Davis and Ian Meginnis. 2019. Testing of the NASA Exploration extravehicular mobility unit demonstration (xemu demo) architecture at the neutral buoyancy laboratory. 49th International Conference on Environmental Systems**].**

[14 Peña-Asensio, E., Sutherland, J., Tripathi, P., Mason, K., Goodwin, A., Bickel, V. T., & Kring, D. A. (2024). Automated astronaut traverses with minimum metabolic workload: Accessing permanently shadowed regions near the lunar south pole. *Acta Astronautica*, *214*, 324-342]

[15] Sargeant, H. M., Bickel, V. T., Honniball, C. I., Martinez, S. N., Rogaski, A., Bell, S. K., et al. (2020). Using boulder tracks as a tool to understand the bearing capacity of permanently shadowed regions of the moon. Journal of Geophysical Research: Planets, 125]

[16 Norheim, J., Hoffman, J., Newman, D., Cohen, T. E., Lees, D. S., Deans, M. C., & Lim, D. S. (2018, March). Architecture of a surface exploration traverse analysis and navigational tool. In *2018 IEEE Aerospace Conference* (pp. 1-11). IEEE].

[17 Lu, S.; Xu, R.; Li, Z.; Wang, B.; Zhao, Z. Lunar Rover Collaborated Path Planning with Artificial Potential Field-Based Heuristic on Deep Reinforcement Learning. Aerospace 2024, 11, 253].

[18 Lavin, A. (2015). Optimized mission planning for planetary exploration rovers. *arXiv preprint arXiv:1511.00195*].

[19 Park, J. M., Hong, S., & Shin, H. S. (2023). Pilot study of low-light enhanced terrain mapping for robotic exploration in lunar psrs. *Remote Sensing*, *15*(13), 3412].

[20 Land, E.H. The retinex theory of color vision. Sci. Am. 1977, 237, 108–129

[21Rasheed, M. T., Shi, D., & Khan, H. (2023). A comprehensive experiment-based review of low-light image enhancement methods and benchmarking low-light image quality assessment. *Signal Processing*, *204*, 108821].

[22]Wang, W., Wei, C., Yang, W., & Liu, J. (2018, May). Gladnet: Low-light enhancement network with global awareness. In *2018 13th IEEE international conference on automatic face & gesture recognition (FG 2018)* (pp. 751-755). IEEE.

[23] D. T. Dang-Nguyen, C. Pasquini, V. Conotter, and G. Boato, “Raise: a raw images dataset for digital image forensics,” ACM Multimedia Systems Conference, pp. 219–224, 2015].
[24]Loza, A.; Mihaylova, L.; Canagarajah, N.; Bull, D. Structural similarity-based object tracking in video sequences. In Proceedings of the 2006 9th International Conference on Information Fusion, Florence, Italy, 10–13 July 2006; pp. 1–6. 53. Pire, T.; Fischer, T.; Castro, G.; De Cristóforis, P.; Civera, J.; Berlles, J.J. S-PTAM: Stereo parallel tracking and mapping. Robot. Auton. Syst. 2017, 93, 27–42]
[25] Pire, T.; Fischer, T.; Castro, G.; De Cristóforis, P.; Civera, J.; Berlles, J.J. S-PTAM: Stereo parallel tracking and mapping. Robot. Auton. Syst. 2017, 93, 27–42]
[26] Park, J.-M.; Hong, S.; Shin, H.-S. Experiment on Low Light Image Enhancement and Feature Extraction Methods for Rover Exploration in Lunar Permanently Shadowed Region. KSCE J. Civ. Environ. Eng. Res. 2022, 42, 741–749
[27] Park, J.-M.; Hong, S.; Shin, H.-S. Pilot Study of Low-Light Enhanced Terrain Mapping for Robotic Exploration in Lunar PSRs. Remote Sens. 2023, 15, 3412].
[28] Schlüter, L.; Cowley, A. Review of techniques for In-Situ oxygen extraction on the moon. Planet. Space Sci. 2020, 181, 104753],